

Mechanism of chemical doping in electronic-type-separated single wall carbon nanotubes towards high electrical conductivity

Electronic Supplementary Information

Ivan Puchades, Colleen C. Lawlor, Christopher M. Schauerman, Andrew R. Bucossi, Jamie E. Rossi, Nathanael D. Cox, Brian J. Landi*

Rochester Institute of Technology, 1 Lomb Memorial Drive, Rochester, NY 14623, USA.

Surface morphology of as-produced and purified films - SEM

The surface morphology of the as-produced and the purified electronic-type-separated SWCNT thin-films can be observed in the SEM micrographs presented in Figure S1 for each electronic-type. There was no appreciable difference observed in the morphology of these thin-films before and after the purification step.

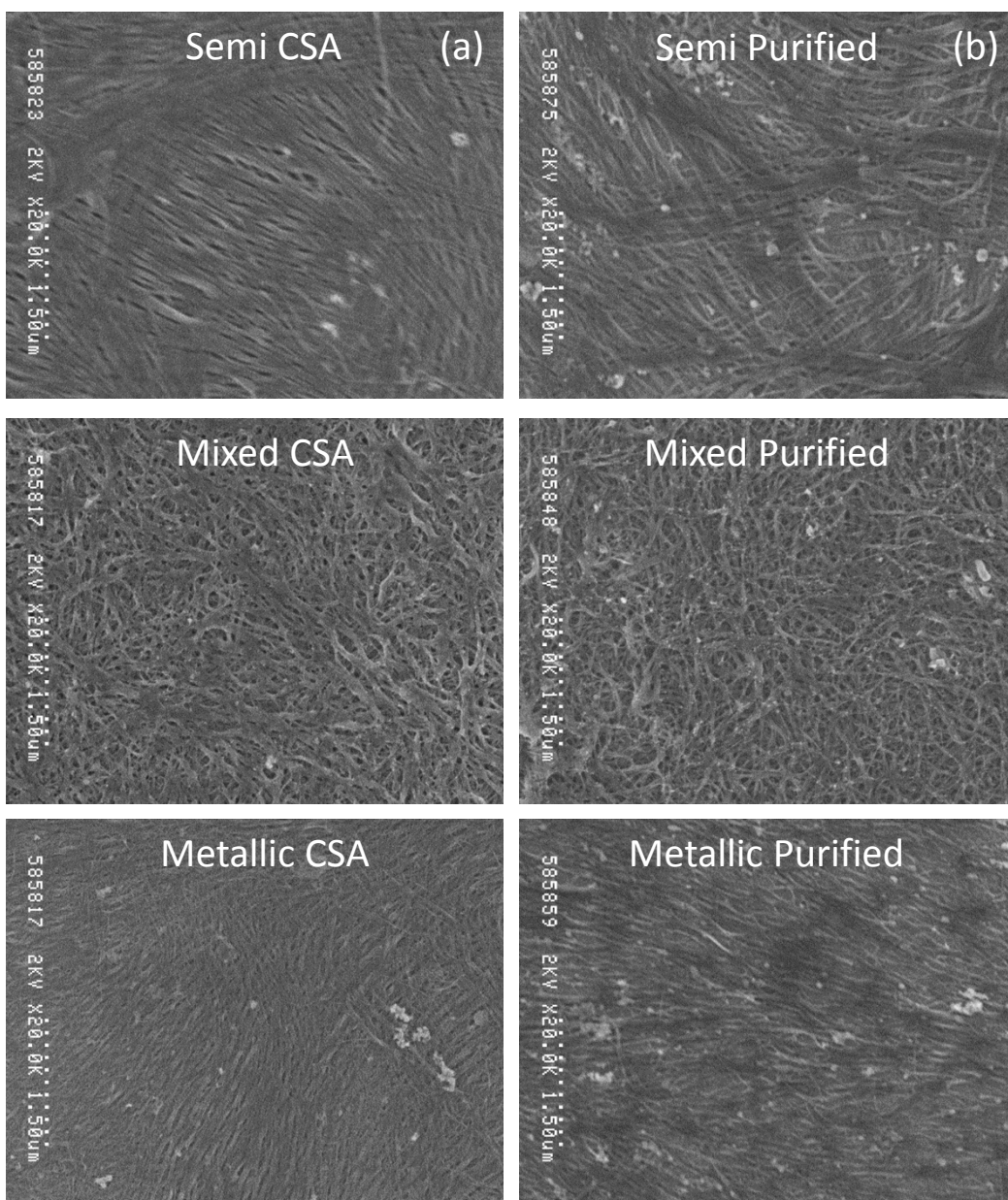


Figure S1. SEM of electronic-type-separated SWCNT thin-films: (a) as-produced, and (b) after purification. There is no appreciable difference in thin-film morphology observed through SEM.

Optical absorbance spectra of purified and doped electronic-type-separated SWCNT thin-films

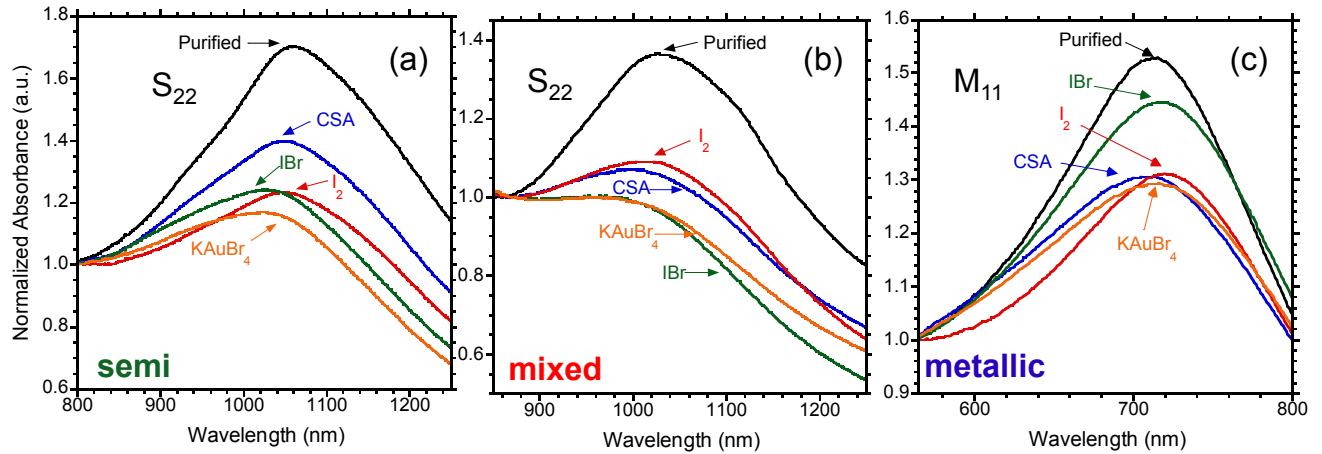


Figure S2. Detail of the normalized optical absorbance spectra of the purified SWCNT thin-films, (a) S_{22} -peak of semi, (b) S_{22} -peak of mixed, (c) M_{11} -peak of metallic, compared to spectra obtained after doping with CSA, I_2 , IBr, and $KAuBr_4$.

Figure S2 compares the relative peak intensities of the optical absorbance for the S_{22} peak for semi and mixed SWCNT thin-films and the M_{11} peak for metallic SWCNT thin-films. A general trend can be observed where the dopants that result in the greatest change in electrical conductivity also exhibit the greatest reduction in absorption peak intensity. For example doping semi SWCNTs with $KAuBr_4$ results in the highest electrical conductivity and greatest S_{22} peak quenching. There can be variation in the optical absorbance peak intensity due to differences in the morphology of doped SWCNT thin-films, which may explain the inconsistent trends with the I_2 doping since it was vapor deposited and could have spatial non-uniformity or light scattering characteristics of the dopant.

Raman spectra of purified and doped electronic-type-separated SWCNT thin-films

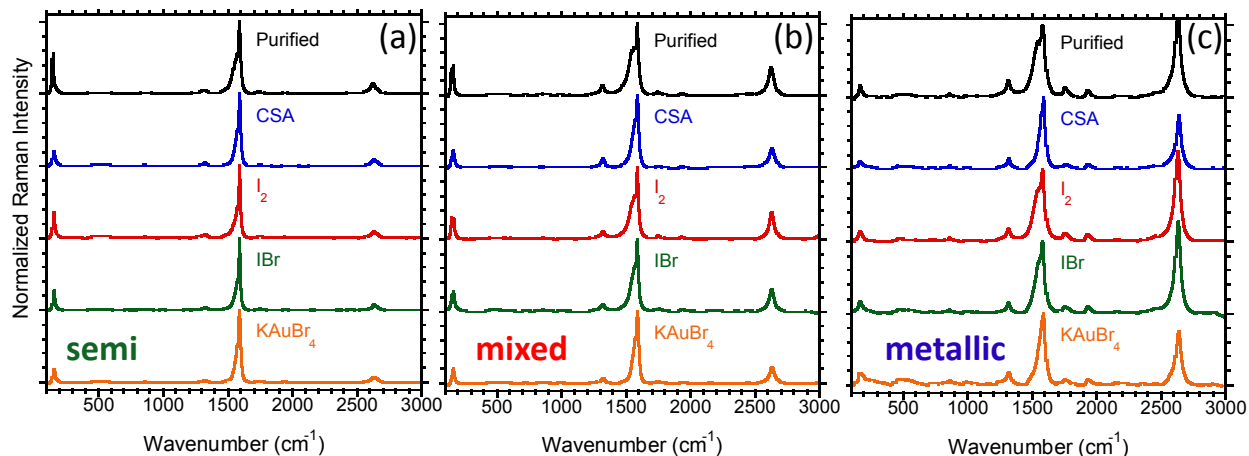


Figure S3. G-peak-normalized Raman spectra of the purified (a) semi, (b) mixed, and (c) metallic SWCNT thin-films, compared to spectra obtained after doping with CSA, I₂, IBr, and KAuBr₄.

The full Raman spectra of the purified and doped electronic-type-separated SWCNT thin-films are shown in Figure S3. These spectra were collected after doping the thin-films. The purified spectra exhibit a clear modulation of the G' peak intensity among the different electronic-type-separated thin-films, with metallic SWCNT thin-films showing the largest G'/G peak ratio and semi SWCNT thin-films showing the smallest. Dopants also modulate the intensity of the G' peak, as shown in the main document, by lowering the G'/G peak intensity and shifting the location of the G' peak when the SWCNTs are doped.

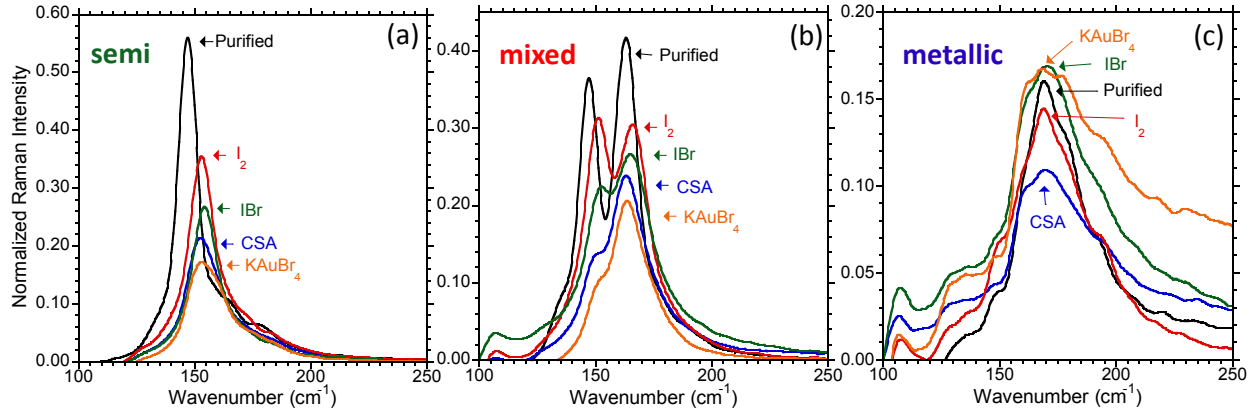


Figure S4. Detail of the G-peak-normalized Raman RBM band of purified and doped (a) semi, (b) mixed, and (c) metallic SWCNT thin-films.

Figure S4 presents the G-peak-normalized Raman radial breathing mode (RBM) band of purified and doped electronic-type-separated SWCNT thin-films after doping. When doped, semiconductor SWCNTs experience a resonance suppression as seen in Figure S4(a). The Raman RBM peak intensity diminishes indicating dopant strength with the following increasing order: I_2 , IBr, CSA, and $KAuBr_4$. The mixed SWCNT thin-films show a bimodal RBM peak as seen in Figure S3(b), which correlates to contribution from both the semiconducting (145 cm^{-1}) and metallic (170 cm^{-1}) SWCNTs. As the mixed SWCNT thin-films are doped, the intensity of both peaks decreases, however, the rate of suppression is greater for the semiconducting region compared to the metallic region. The resonant signal of the semi SWCNTs has been suppressed in the same dopant-strength order as observed for the phase pure semiconducting SWCNTs. On the other hand, the resonant signal of the metallic SWCNTs that compose the mixed SWCNT thin-films is only slightly quenched, indicating that the dopants studied in the current work do not dope metallic SWCNTs as effectively as semiconducting SWCNTs. This observation is confirmed by Figure S4(c), where the Raman spectra of the metallic SWCNT thin-film do not indicate any appreciable changes in the RBM region after doping.

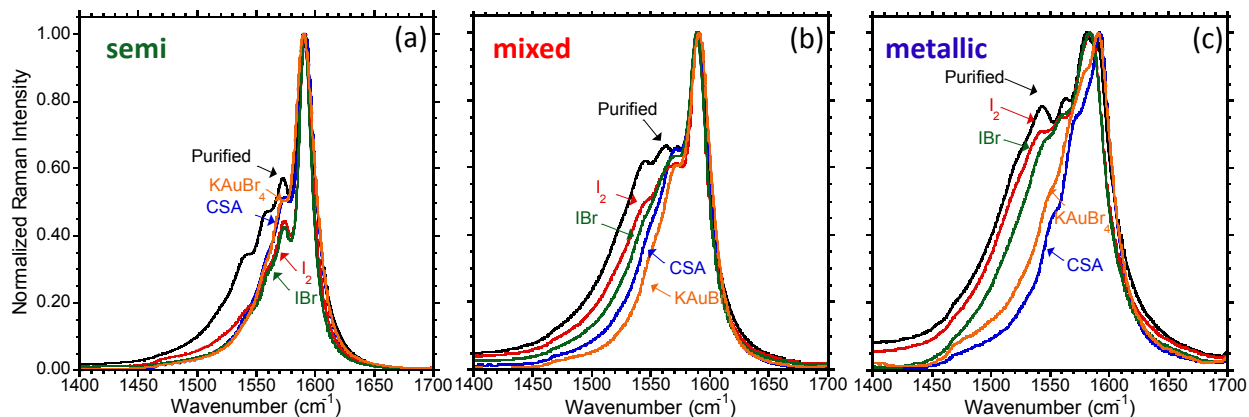


Figure S5. Detail of the G-peak-normalized Raman G-band of purified and doped (a) semi, (b) mixed, and (c) metallic SWCNT thin-films.

Figure S5 shows the G-peak-normalized Raman G-band of purified and doped electronic-type-separated SWCNT thin-films. Changes in the line shapes and peak intensities of the G-band, and in particular the Breit-Wigner-Fano (BWF) line shape, are characteristic of metallic SWCNT thin-films and attributed to optical plasmon corresponding to the tangential motion of the electrons on the SWCNT surface. The suppression of the BWF line shape is observed in both the mixed and metallic SWCNT thin-films. As the dopants oxidize the SWCNT thin-films, there is a reduction in the number of electrons, and the suppression of the BWF line shape increases with increasing dopant strength ($\text{KAuBr}_4 \geq \text{CSA} > \text{IBr} > \text{I}_2$). The extent to which the dopants affect the BWF line shape in the mixed and metallic SWCNT thin-films is based on dopant strength, whereas all dopants seem to affect the semi SWCNT thin-films similarly.

Relative change in conductivity based on dopant and electronic-type

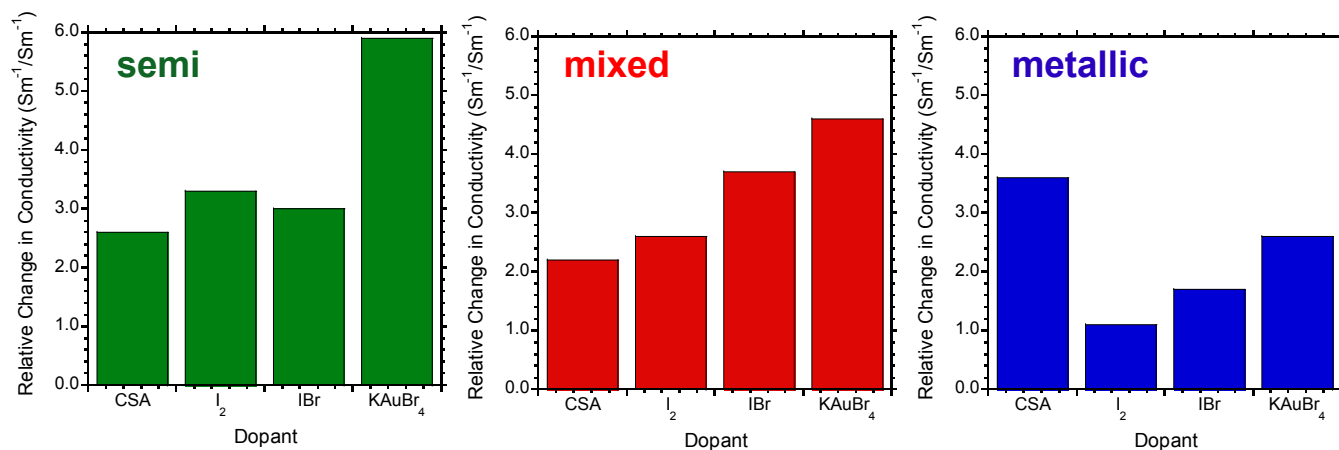


Figure S6. Relative change in conductivity based on dopant and electronic-type.

Figure S6 shows the relative change in electrical conductivity of the doped electronic-type separated thin-films. The bar graphs show that the relative change in conductivity for the mixed SWCNTs is approximately averaged between the pure semi and metallic results for dopants like KAuBr_4 and I_2 . Since the network transport in mixed SWCNT electronic-types is dominated by contact resistance effects between electronic type-pure SWCNTs (see Topinka et. al, 2009, reference 38), the subtle changes in the inter-SWCNT transport may influence the differences for CSA and IBr.

Time dependent measurements

The dopant stability over time was characterized in two different ways for semiconductor SWCNT thin-films and metallic SWCNT thin-films. Optical absorbance was used as an indication of dopant stability on semi SWCNT thin-films due to the large sensitivity to dopants, which is demonstrated in the main text during the analysis of the S_{11} and S_{22} peaks. On the other hand, Raman spectroscopy was used as an indication of dopant stability in metallic SWCNT thin-films

due to the little effect that dopants had on the optical spectra M_{11} peak obtained through absorbance spectroscopy.

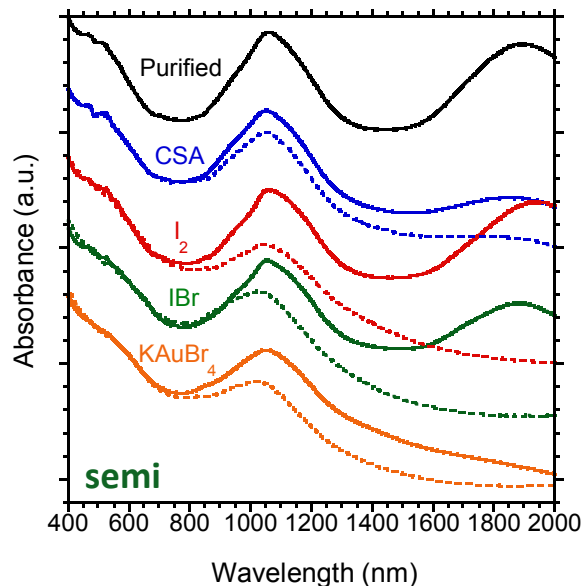


Figure S7. Optical absorbance spectra of doped semi SWCNT thin-films after doping (dashed lines), compared to 40 days after doping (solid lines).

Figure S7 shows a comparison of the optical absorbance spectra of the semi SWCNT thin-films immediately after doping (dashed lines) and 40 days after doping (solid lines), as a qualitative indicator of the doping level. The S_{11} peak of the semi SWCNT thin-films doped with I_2 and IBr has recovered to values of the purified thin-film. On the other hand, the CSA-doped thin-film show a modest recovery of the S_{11} peak, while the $KAuBr_4$ doped thin-film remained completely quenched.

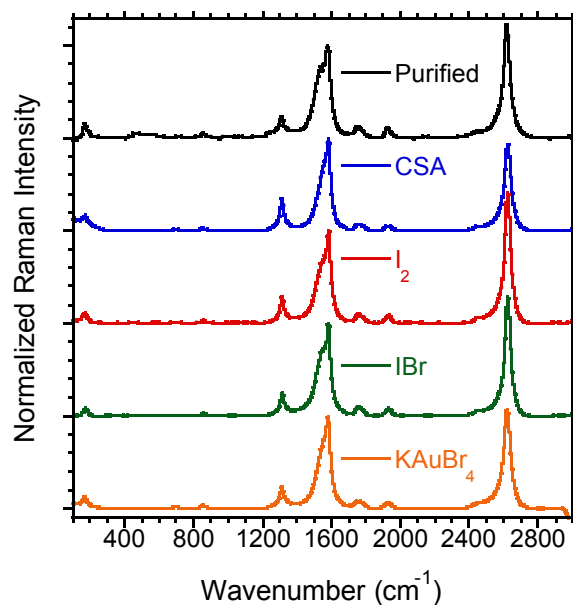


Figure S8. G-peak-normalized Raman spectra of purified and doped SWCNT metallic thin-films 40 days after doping.

Correspondingly, Raman spectroscopy was used on metallic SWCNT thin-films as an indicator of doping stability. Figure S8 shows the full Raman spectra of the metallic SWCNT thin-films 40 days after doping. All spectra were normalized to the G peak maximum intensity. Differences seen in the D peak intensity 40 days after doping, when compared to the films immediately after doping, are partly due to the recovery of the BWF feature of the G-band, as seen in Figure S9. There is an exception with the behavior of CSA-doped film, where the D-peak increases more significantly than what should be expected for the recovery of the observed BWF feature. This may indicate that defects are created as the CSA interacts with water vapor in the ambient over time. Similarly, the D-band of the metallic I₂-doped SWCNT thin-films increases as its BWF feature decreases. The explanation for this could be the residual disorder observed as the I₂ dopant is removed from the film.²² The increase in defects observed in these two thin-films may be partially responsible for the decrease in their electrical conductivity.

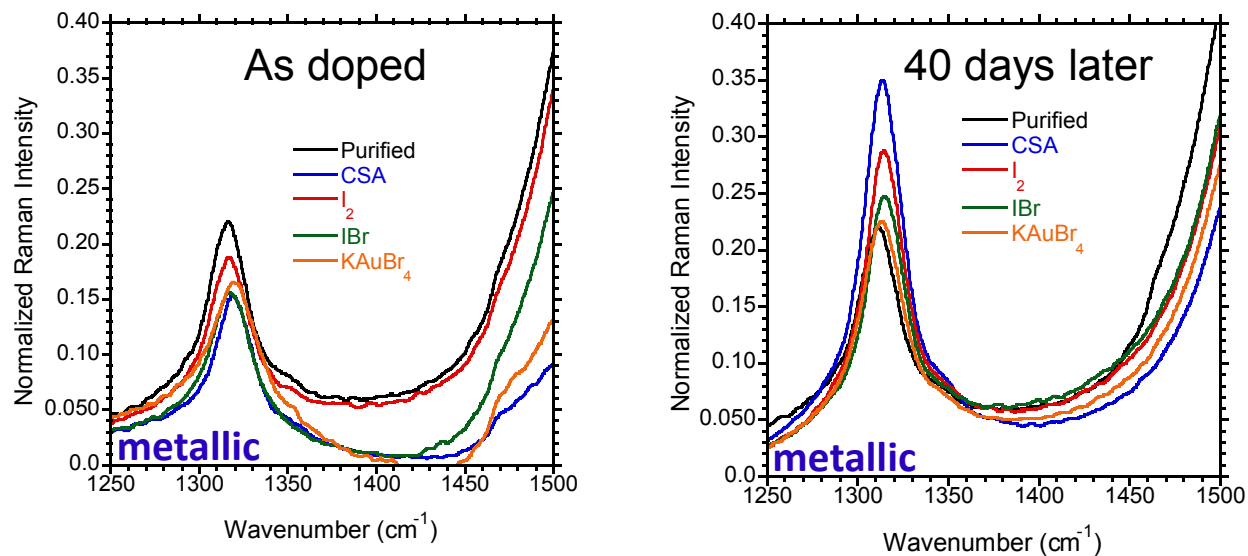


Figure S9. Comparison of G-peak-normalized Raman D-band of purified and doped metallic thin-films as doped and 40 days after later.

Figure S10 shows an overlay of the G' peak for the purified and doped metallic SWCNT thin-films after exposure to CSA, I_2 , IBr, and $KAuBr_4$, respectively. The change in the G' peak relative to the G peak yields important information about the doping stability. Compared to the purified metallic SWCNT thin-film, there is very little change observed in the normalized G' peak after doping with I_2 and IBr, and remains unchanged after 40 days in ambient conditions. In contrast, the G' peak of the metallic SWCNT thin-films doped with CSA and $KAuBr_4$ show both a shift in position and increase in intensity towards the purified control film, thus indicating that the effects of these dopants have been reversed.

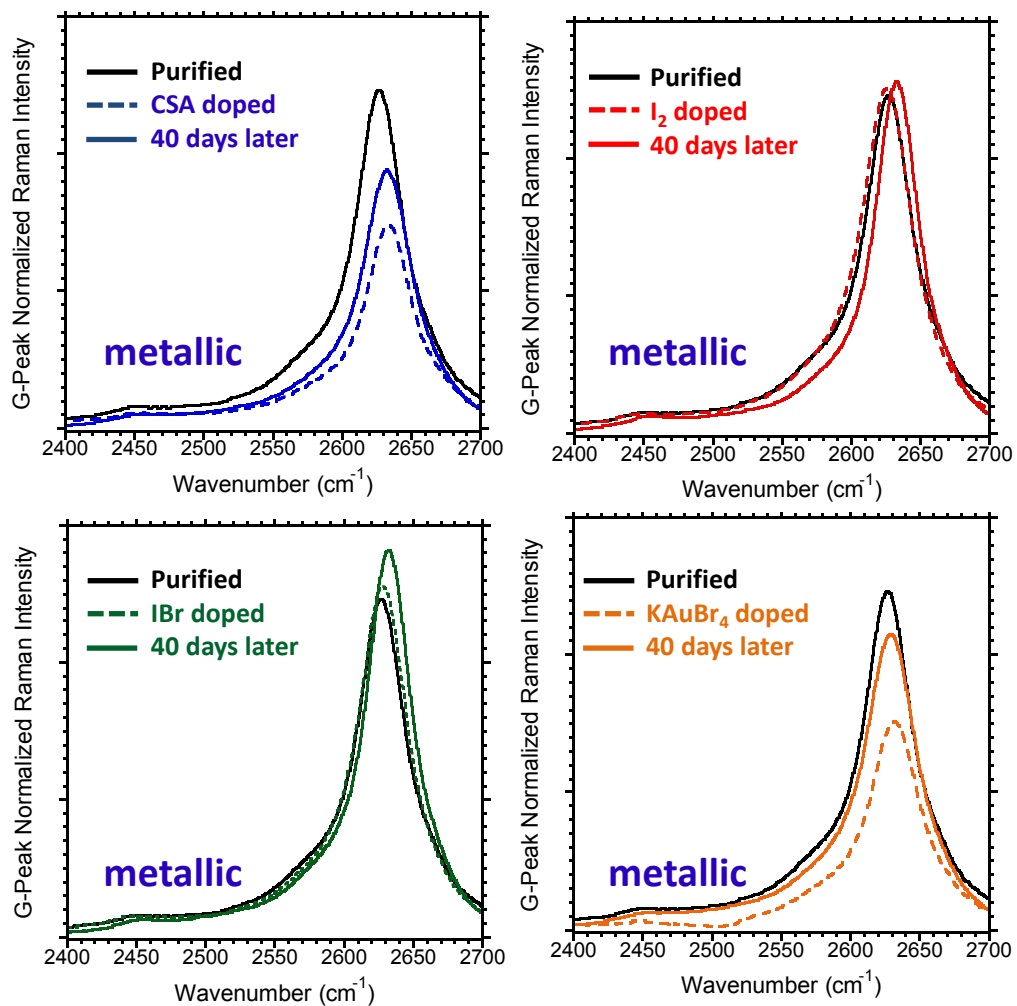


Figure S10. Detail of normalized Raman G'/G band of purified and doped SWCNT metallic thin-films doped with (a) CSA, (b) I₂, (c) IBr, and (d) KAuBr₄ comparing the intensity and position of the peak immediately after doping and 40 days after doping.